RESEARCH WAVE OCEAN ENERGY

CONVERTER USING LINEAR GENERATOR

Phung Van Ngoc[1]; Nguyen Chi Cuong[1]; Nguyen Minh Tuan[1]

1. *Hanoi University of Scientist anh Technology No1 - Dai Co Viet, Hai Ba Trung, Hanoi,10000, Vietnam*

Email: phungthanhngoc@gmail.com

Abstract: *This paper presents results of numerical simulation for a wave energy converter using linear permanent magnet generator. Using a linear permanent generator has the advantages of simple structure, minimizing the mechanical loose… On the basic mechanics model, a system of equations describing the operation of the device under linear potential wave was obtained. The magnetic field in generator was calculated by FlexPDE software. The system of movement equations was numerically solved with Matlab. Various calculations were performed with the different parameters of wave conditions and device's structures to determine the device's configuration for a 300W output power under wave condition in the South-Central offshore of Vietnam. The results also show potential of developing the wave energy conversion to meet the energy demand in some coastal and island regions of Vietnam.*

Keywords: *wave ocean energy; buoys; generator; rotor; converter*

1. Introduction

1.1. Ocean wave energy

In terms of fossil energy resource depletion and sustainable development, the use of renewable energy, including wave energy is inevitable. The global power potential represented by waves is estimated to be 1–15 TW [1]. Technically, the potential available in Sweden is estimated to 5–10 TWh annually which can be compared to Sweden's total electric energy consumption during one year, 144 TWh [1].

In Vietnam, according to the latest studies, the total wave power in the coast zone is about 58677.02 MW while the total electric power generation capacity of Vietnam in 2010 was 12200.00 MW [2, 3]. The region has great potential for wave energy in Vietnam is South-Central offshore. The annual average wave energy flux for this region is over 30kW/m and reaches the maximum value of about 100 kW/m in December. This is a good energy resource to meet the energy demand of the development.

1.2 Wave energy conversion technologies

Up to day, different types of wave energy conversion principles are illustrated, which have carefully been documented and presented as in Fig. 1 [4]. So far most researchers have concentrated on the hydrodynamic aspects of different converters. The two best known concepts are the IPS buoy [5] and the AquaBouy [6, 7]. These devices all require an intermediate mechanical structure to transform the kinetic energy of the buoy to that compatible with the conventional turning generator, such as pump and turbine systems. However, the complexity in structure increases mechanical energy loss, and it is very hard to get the generators and related accessories available to fit the device's characteristics. They cause reliability problems when operating in extreme marine environment conditions and this is the biggest barrier to the success of the project to manufacture wave energy converter in real field conditions [7].

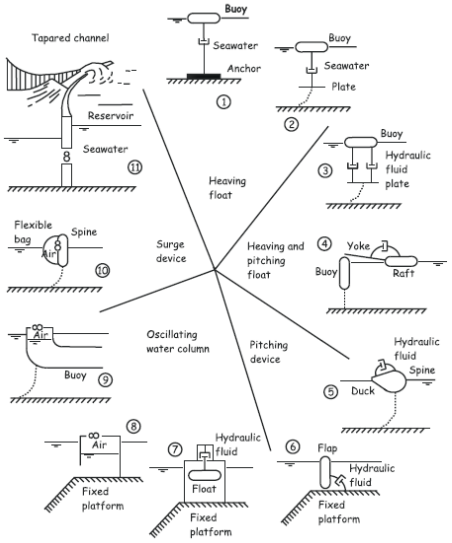

Fig. 1 Illustration of different principles for wave energy absorption

Recently, a number of different working principles to convert wave energy using linear generator have been presented and described [7]. Particularly, the direct conversion using point absorbed and three-phase synchronous three-slide linear generator have been simulated for 10kW units [7]. This structure has the advantage of simple, without many intermediate structures, less mechanical energy loss. Permanent magnet generator helps more dependable operation in hard conditions of the marine environment [6-7].

For starting develop wave energy convertor that is suitable with wave conditions and using purposes in Vietnam, this study deals with a 300W wave energy convertor. This device consists of a buoy connects directly with a linear permanent magnet generator placed at the sea bottom. The generator consists of a two-slide piston with surface mounted permanent magnets. The piston is connected to a buoy by a robe. Stator is situated outside piston with symmetric winding. Reciprocal movements of the piston induce currents in stator winding (Fig. 2a).

2. Concept model and modeling

2.1 Concept model

The concept and operation of the device are described in Fig. 2a. The piston is covered with rows of permanent magnets of alternating polarity. The magnet rows are separated with aluminum spacers. The stator is made of laminated electrical non-oriented steel sheets and isolated copper conductors. The conductors are wound in slots (holes) in the stator steel and forms closed loops or coils. When the buoy oscillates in heave mode under wave forces, it makes piston move relative to the stator. Reciprocate movements of the piston induce currents in stator winding. The current in turn affects the piston with Lorentz force opposite to the direction of motion. The oscillating model of the device is presented in Fig. 2c.

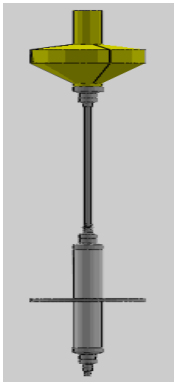

a) Concept model.

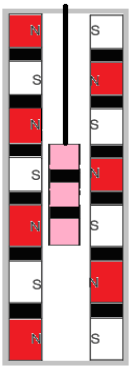

b) stator and "rotor" of generator.

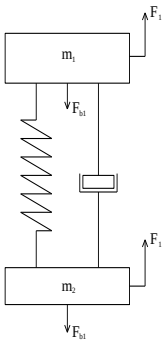

c) Oscillating model.

Fig 2: Device's model.

2.2. Governing equations

- Linear wave theory

Ocean waves are very complex. In this study, the analysis is carried out for the linear wave theory only. Then the wave equation has the form:

$$\eta(t) = \eta_a \cos(\omega t - kx) \qquad (1)$$

In which, $\eta(t)$ is the surface water displacement related to still water level, η_a is the wave amplitude, ω is angular frequency, k is wave number.

- Buoy's motion

We select a point-absorbed system of mass m and model its response to monochromatic wave extinction. The dynamic equation of motion for a heaving structure is [12]

$$\begin{aligned} m_b\,\ddot{s}(t) + S_b s(t) &= F_{w,b}(t) + F_{f,b}(t) + F_u(t) + F_c(t) + F_m \\ m_b\,\ddot{s}(t) &= F_{w,p}(t) + F_{f,p}(t) - F_u(t) - F_c(t) - F_m + F_{drag}(t) \end{aligned} \qquad (2)$$

where s_b is the vertical distances of displacement from equilibrium of the buoy, m_{b1} is the mass of the buoy, $F_{e,b}(t)$ is the excitation force, $F_{r,b}(t)$ is radiation force, $F_{b,b}(t)$ is the net buoyancy force, $F_{b,drag}$ is the drag force, $F_{b,f}$ is the friction loss force, $F_{b,u}$ is the electromagnetic load force from generator.

These equations can be reorganised as follows.

$$\begin{aligned} m_b + m_{r,11}(\infty))\dot{u}_b(t) + m_{r,12}(\infty)\dot{u}_p(t) &= g_1(t) \\ m_{r,21}(\infty)\dot{u}_b(t) + (m_p + m_{r,22}(\infty))\dot{u}_p(t) &= g_2(t) \end{aligned} \qquad (3)$$

When the expressions for the radiation forces given in equation (3) have been used, and the following functions have been introduced to increase the readability.

$$\begin{aligned} g_1(t) &= F_{e,b}(t) - k_{11}(t)u_b(t) - k_{12}(t)u_p(t) \\ &- R_{f,b}u_b(t) - S_b s_b(t) + F_u(t) + F_c(t) + F_m \\ g_2(t) &= F_{e,p}(t) - k_{21}(t)u_b(t) - k_{22}(t)u_p(t) \\ &- R_{f,p}u_p(t) - F_u(t) - F_c(t) - F_m + F_{drag}(t) \end{aligned} \qquad (4)$$

By further manipulation the equations of motion can be written as the following system of equations:

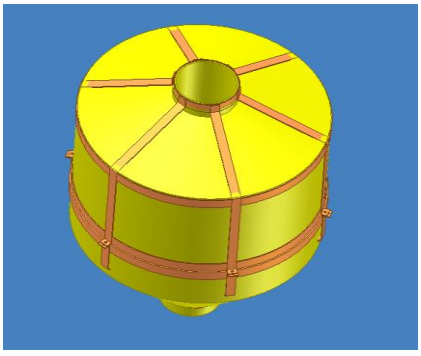

Fig. 3 The concept device's model.

3. Point wave absorber model

The point wave absorber model contains a float and a reaction part that includes a central column and a reaction plate. For extreme wave conditions, we assumed the absorber to be locked, and we performed the numerical study assuming all the parts are moving together as a single rigid body.

We first designed the model using SolidWork, and then further modified the geometry in the numerical modeling by keeping the center of buoyancy, B, as close as to the original SolidWork design. The model properties and the dimensions are shown in Tab. 1 and (Fig.2, Fig.3), respectively, where G is the center of gravity, and the metacentric M is calculated by following

$$BM = I / \forall$$
$$GM = OG - OB + BM \quad (5)$$

where O is located at the intersection of the mean free surface and the longitudinal axis of the FPA, I is the area of inertia, and $\forall$ is the displacement of the model.

Modeling rans method

We applied a finite volume method-based RANS model (StarCCM+) for solving the details of the unsteady incompressible flow field around the FPA. The continuity equation and the Navier-Stokes equations are given as.

$$\nabla . U = 0,$$
$$\rho(U_t + U.\nabla U) = \nabla p + F_b + \nabla T \quad (6)$$

where ρ is the water density, U is the flow velocity vector, and U_t is its time derivative, F_b is the body force vector (e.g., gravity), and T is the stress tensor.

The governing equations are discretized over the computational domain and are solved using a transient SIMPLE for the pressure–velocity coupling.

The set of linear equations is solved through the use of an algebraic multigrid method. A k-ω SST turbulence model is applied with a two-layer all y+ wall treatment model, and the unsteady simulation is performed using a second order implicit scheme for time marching. The water free surface is captured using a volume of fluid (VOF) method, and a morphing model is adopted to move the mesh, where the cell movement and its deformation are taken into account in the momentum equation using an arbitrary Lagrangian-Eulerian method.

Absorber response calculation

The translation and rotation of the body of the body (Fig. 2) is calculated by solving the equation of motion after the excitation force is obtained, and the equation of motion calculation is coupled with the RANS simulation. The translation and the rotation of the body at the center of gravity are solved following

$$F = m_b a_t$$
$$M = I_g a_\Omega + \Omega \times I_g \Omega \quad (7)$$

where m_b is the mass of the body, a_t is the acceleration vector for the translation, Ω and a_Ω are the angular velocity and acceleration vectors, I_g is the moment of inertia tensor at the center of gravity, F and M are the resulting force and moment acting on the body, including the buoyancy force, wave load and the weight of the body. The corresponding translational and rotational motions are calculated by integrating the accelerations over time, and the equation of motion is coupled with the RANS method through iterations.

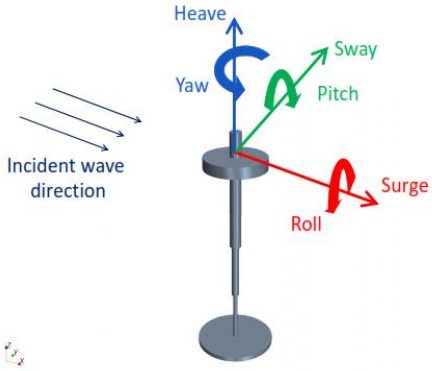

Fig.4 The transliton and rotation of the body

Numerical wave tank settings

The domain and the domain boundaries of the numerical wave tank are plotted in Fig. 4, where the water depth is 70 m. To reduce the size of the problem, a symmetric boundary is applied along the *x*-*y* plane. The given computational domain is 100 m wide (0m≤*y*≤100m); 170 m high (-70m≤*z*≤100m); 7 wavelengths long (-2λ≤*x*≤5λ) in the regular wave analysis and 9 wavelengths long (-2λ≤*x*≤8λ) in the irregular wave analysis. The wall width to FPA diameter radius is around. The effect of wave reflection from the side wall is assumed to be small in this study. However, more studies need to be performed to quantify the impacts. The incident wave condition is specified at the inflow boundary, and a sponge-layer method is applied by placing a damping zone (2λ in the wave propagation direction) in front of the down wave boundary in order to absorb the outgoing and reflecting waves without creating additional numerical disturbance. Note that the sponge-layer damping zone method has been tested. It successfully absorbs the waves in a numerical wave tank without the presence of the absorber.

Mooring configuration

The FPA is connected to a mooring system to

contain its horizontal and rotational motions. We are not trying to model a particular mooring system in this study. For design and optimization purposes, we use OrcaFlex to conduct the mooring line configuration study, which is a fully 3D time domain fluid and structural dynamic modeling tool. It has widely been used for modeling the dynamics of the offshore systems. The excitation forces on the absorber include the buoyancy force and the hydrodynamic wave loads that are calculated through the use of Morison's equation. The dynamics of the absorber and the mooring system are then modeled using a finite element method. The drag and added-mass coefficients for the Morison's equation are given based on. Note that the effects of wave diffraction and radiation as well as the nonlinear interaction between waves and the floating body are not considered in the modeling. Although OrcaFlex has its limitations, it can provide us first-cut results in a very short time.

Based on the approach used by Fitzgerald and Bergdahl, and after running a series of OrcaFlex simulations with various mooring configurations, we present an "acceptable" mooring design (Fig. 4), for which the deviation of pitch is less than 25 degrees. The FPA model is connected to eight mooring lines that are divided into two layers. Each layer has four lines in the configuration of a cross, and each mooring line is connected to a spring system. The spring stiffness is equal to 160kn/m and is determined based on a series of OrcaFlex runs.

In the RANS simulation, the sway, roll and yaw motions are constrained, and the FPA is only allowed to move freely in surge, heave, and pitch. The mooring system is designed based on the one used in the OrcaFlex modeling. Given that a symmetry boundary is applied, only four mooring lines are specified along the symmetry boundary in the RANS simulation (Fig. 5).

Rans simulation

To model the details of the flow around the FPA, including wave overtopping and the nonlinear interaction between waves and the moored FPA, we utilized the RANS method. The FPA wave energy system is analyzed in both regular and irregular waves, where a 5th-order Stokes wave with a height of 10m is applied for the regular wave study and a JONSWAP spectrum wave is applied for the irregular analysis.

Meshing

As shown in Fig. 5, the mesh is finer near the free surface in order to capture the wave dynamics and has a higher resolution around the FPA to model the details of the flow around it and its interaction with waves. In addition, prism-layer cells are placed along the FPA surface so that $y+$ satisfies the turbulence model requirement.

The grid size Δx (in the wave propagation direction) is adjusted with the incident wavelength, and it is smaller than $\lambda/80$. The grid size Δz (in the vertical direction) near the free surface is in the range between H/10 and H/20, where H is the wave height. The total number of cells is on the order of 0.7 million for the regular wave analysis and 1.5 million for the irregular wave analysis.

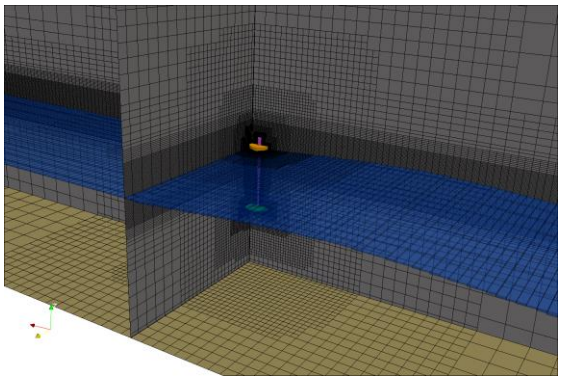

Fig.5 Mesh around the point wave absorber model

In addition, a very small time step is utilized to avoid highly distorted cells, created by the morphing model due to the large movement of the FPA at each time step. The time step size is also given based on the incident wave period, and it is approximately T/300 in the regular wave analysis and $T_p/600$ in the irregular wave analysis, where T and T_p are the period and the peak period for the regular and irregular waves, respectively.

Long linear wave comparison

For long linear waves, the comparison of the heave and surge motions of the FPA are plotted in Fig.6, which shows the results from the RANS method and OrcaFlex are in good agreement. When the wave is linear and the wave period is large, the vertical component of the excitation force is dominated by the buoyancy force, and the horizontal component is determined by the hydrodynamic wave loads. The buoyancy force is proportional to the immersed volume of the FPA, and the hydrodynamic wave loads in the horizontal direction can be calculated accurately through the use of Morison's equation because the size of the FPA is much smaller than the incident wavelength and wave overtopping barely occurs.

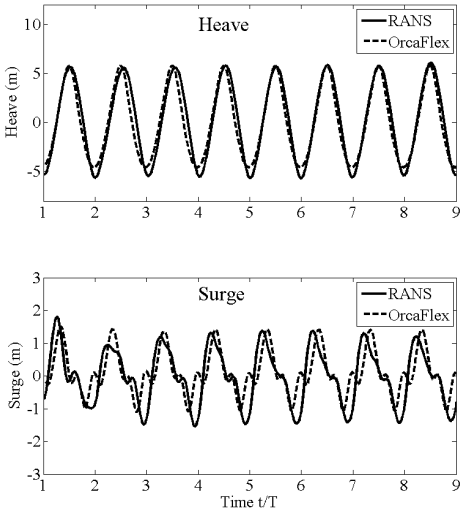

Fig.6 Comparison of the heave and surge motions from rans and OrcarFlex

Regular wave analysis

The response amplitude operators (RAOs) obtained from OrcaFlex only have good agreements with those obtained from the RANS method when the wave period is larger than 17 sec (Fig. 7). When the wave period is small, the RAOs predicted by the RANS method are smaller than those predicted by OrcaFlex. As opposed to the OrcaFlex results, the RANS solutions do not experience a resonance period in heave, at least within the range of wave periods that are studied. As shown in the heave motion of the FPA generally follows the wave elevation when the incident wave period is sufficiently larger than the body natural period. When incident wave period decreases, the phase shift between the wave elevation and the FPA heave motion increases. As a result, the waves are more likely to overtop the FPA model (Fig. 4), particularly in extreme wave scenarios, where a wave with a height of 10 m is generally nonlinear when the wave period is smaller than 11 sec. In addition, flow separation is observed around the float and the reaction plate in the RANS simulation. These nonlinear effects generally provide additional damping that constrains the FPA motions.

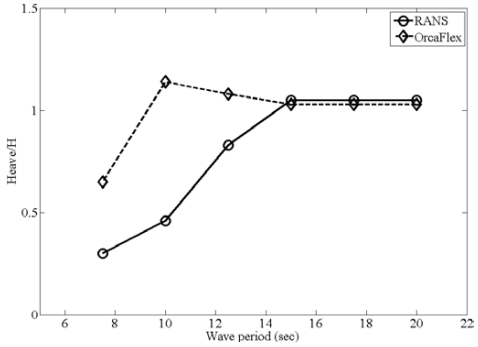

Fig.7 Comparison of raos from rans and OrcarFlex

Figure 8 plots the surge and pitch of the FPA in waves. The surge response is in the range between 3 m and 6 m, and the pitch angle is around 5 degrees. Both the surge and the pitch increase slightly as the wave period decreases.

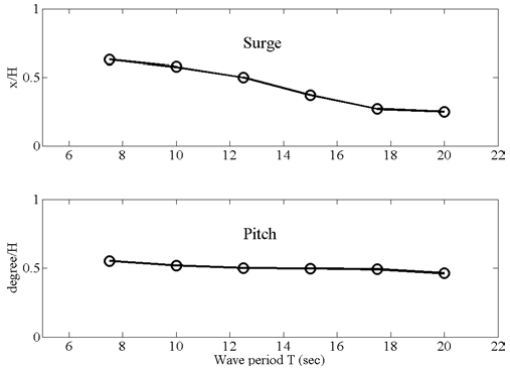

Fig.8 Surger and pitch motions of the FPA model from rans simulations

Figure 9 shows the hydrodynamic pressure distribution near the FPA model at a time instant of t/T=7.65. Note that the absorber is subject to a wave at its peak at t/T=10.49, and at its trough at t/T=9.99. Because the motion of fluid particles decreases rapidly with increasing depth below the free surface, the hydrodynamic wave impact on the float is more significant than that on the reaction plate.

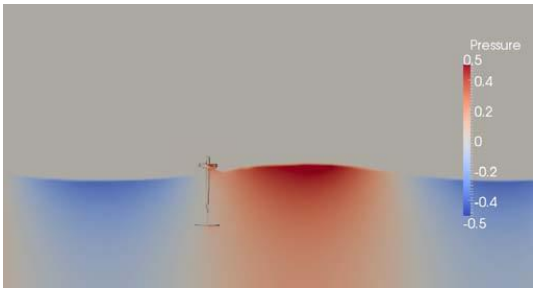

Fig.9 Hydrodynamic pressure contour around FPA

The corresponding horizontal and vertical forces, including the buoyancy force, wave impact, and the weight of the FPA device are plotted in Fig. 14. Given that the fluid particle velocity is proportional to the incident wave frequency, the forces increase as the incident wave period decreases as expected. The forces on the FPA body under extreme wave conditions are useful information for further cost assessment.

Irregular wave analysis

In our irregular wave analysis, we only present a scenario where the FPA is modeled using a JONSWAP spectrum wave with a significant wave height of 10 m and a peak period of
17.5 sec. The corresponding hydrodynamic response histories from the RANS method are shown in Fig.

15. The maximum heave motion is on the order of the maximum wave height. We plan to conduct a more detailed analysis with a longer period of simulation and various wave conditions in the future.

4. Discussions

As the wave period decreases, the phase shift between the FPA heave motion and the wave elevation increases. Therefore, the nonlinear interaction between waves and the FPA device becomes more significant, especially in small wave period and large wave height scenarios. As a result, the additional damping forces, including those due to flow separation and wave overtopping, limit the motion of the FPA, particularly under the extreme wave conditions.

The Morison's equation prediction is expected to be applicable when the wave is linear. However, for some linear wave scenarios, the OrcaFlex results are deviated from the RANS simulations, as shown in Fig. 9. In addition to the aforementioned nonlinear effects, the relationship between the buoyancy force and the hydrodynamic wave loads and the feasible values of the added-mass and damping coefficients for predicting the excitation force of this particular FPA geometry require further investigation, particularly in the body axial direction. A more rigorous method is to compute the hydrodynamic coefficients through the use of a potential flow method.

Although using OrcaFlex for predicting the FPA motions has its limitations, OrcaFlex is still an efficient numerical tool that provides us with a very useful first-cut analysis, particularly for small amplitude linear wave scenarios. The computational cost for running such a design and optimization tool is small. On the other hand, under extreme wave conditions, the hydrodynamics of a FPA is complex. The interaction between waves and the moored FPA is often fully nonlinear, and wave overtopping often occurs. Therefore, the use of RANS models is suggested.

5. Conclusions

In this paper, we presented the results of our study of the hydrodynamics of a moored FPA in extreme wave conditions. We analyzed the baseline mooring configuration using OrcaFlex and modeled the detail of the flow using a RANS method. The study shows that waves often overtop the FPA when the FPA is under extreme wave conditions. The FPA motions are constrained by the effects of viscous damping as well as the nonlinear interaction between waves and the moored FPA. Furthermore, through a few irregular wave simulations, we find that the maximum heave motion of the FPA is on the order of the maximum wave height, although more simulations are needed to confirm this. Overall, we found our mooring line design to be effective. We also found that the Morison's Equation method can be only used for a very few scenarios and with caution for extreme wave scenarios analyses.

6. Acknowledgment

This study is completed with partial funding from the project "Researching, designing and manufacturing a prototype model of a smart source using renewable energy", University of Engineering and Technology, Vietnam National University.

References

1. A. Clement, P. McCullen, A. Falcao, A. Fiorentino, F. Gardner, K. Hammarlund, G. Lemonis, T. Lewis, K. Nielsen, S. Petroncini, P. Schild M.-T. Pontes, B.-O. Sjostrom, H. C. Sorensen, and T. Thorpe. 2002. Wave energy in europe: current status and perspectives. Renewable and Sustainable Energy Reviews, 6:405–431.

2. MOST (Ministry of Science and Technology). 2010. Study on evaluation of potential marine energy sources and propose of exploitation approaches. KC.09.19/06-10 Project report.

3. IMECH (Institute of Mechanics), Vietnam Academy of Science and Technology. 2003. Study on potential use of marine energy sources of Vietnam. Project report.

4. G.M. Hagerman and T. Heller. 1988. Wave energy: a survey of twelve near-term technologies. Proceedings of the international Renewable Energy Conference, pages 98–110. Honolulu, Hawaii, 18-24 September.

5. G. Fredriksson. 1993. Ips wave power buoy. Wave Energy R&D, Cork, Ireland.

6. B-O Sjöström. 1994. The past, the present, and the future of the hose-pump wave energy converter. First European Wave Energy Symposium. Edinburgh.

7. Dang the Ba, Dinh Van Manh and Pham Thi Minh Hanh. 2010. Modeling and Simulation of a Heaving-Buoy Wave-Energy Convertor. International Conference on Engineering Mechanics and Automation (ICEMA 2010). Hanoi, July 1-2, 2010.